Evaluation of Desertification in the Middle Moulouya Basin (North-East Morocco) Using Sentinel-2 Images and Spectral Index Techniques

Mohamed Lamaamri[1*], Nezha Lghabi, AbdelKhalek Ghazi[1], Noureddyne El Harchaoui[2], Mohammed Sarfaraz Gani Adnan [3], Mohammad Shakiul Islam[4]

[1] *Laboratory of Environment, Development and Space Management, Department of Geography, Faculty of Letters and Human Sciences, Ibn Tofail University, Kenitra, 14000, Morocco.

[2] Department of Geography, Faculty of Letters and Human Sciences, University Moulay Ismail, Meknes, B.P.11202, Morocco.

[3] Environmental Change Institute, School of Geography and the Environment, University of Oxford, OX1 3QY, United Kingdom

[4] Department of Geosceineces, Mississippi State University, MS-39762, USA

*Corresponding author(s). E-mail(s): lamaamri.mohamed@gmail.com (+212648461475);

Abstract

This article focuses on the quantitative assessment of desertification in the Middle Moulouya basin located in the North-East of Morocco. Indeed, this study aimed to map the degree of desertification at the level of the basin in 2018 using the Sentinel-2 image. To do this, we have adopted a methodology based on several stages. First, we extracted the spectral indices, in particular, the NDVI, the albedo, the TGSI and the MSAVI. Then, different combinations of these indices were the subject of a linear regression analysis (NDVI–albedo, MSAVI–albedo, albedo–TGSI and TGSI–MSAVI) to use the best correlated combinations to construct the feature space. The results obtained showed that the NDVI–albedo and MSAVI–albedo combinations are the best correlated with respective correlation coefficients of $r = -0.73$ and $r = -0.76$, respectively. As a result, they were used to propose the desertification degree index (DDI) by exploiting the NDVI–albedo and MSAVI–albedo feature spaces. Finally, a desertification map was generated for the entire basin. It has five degrees of desertification (extreme, severe, moderate, low, non-desertification). According to our results, the situation of desertification in the basin is alarming. Indeed, 86.86% of the study area is located in the moderate to extreme desertification class. While only 12.25% and 0.89% fall in the low and no desertification categories, respectively. The MSAVI–albedo model gave a high overall accuracy of 93.75%, so it is perfectly effective for the quantitative analysis and monitoring of desertification at the level of the basin studied.

Keywords: Desertification, NDVI, Albedo, TGSI, MSAVI, Middle Moulouya, Sentinel-2, feature space.

1 Introduction

Globally, desertification is one of the most complex environmental issues (Kosmas et al. 2014), affecting the socioeconomic conditions of millions of people in different regions (Adger et al. 2001; Reynolds et al. 2007). Desertification primarily occurs in arid, semi-arid, and dry sub-humid regions due to various climatic and anthropogenic forcings such as climate change and overexploitation of natural resources (overgrazing, exploitation of natural land for agriculture, deforestation, etc.) (UNEP 1994; Brandt and Thornes 1996; Yassoglou and Kosmas 2000; UNCCD 2004; Yu et al. 2018). This natural hazard can lead to extreme land degradation, loss of biodiversity, habitat loss, species endangerment, and loss of productivity of lands (Verbist et al. 2010; Herrmann et al. 2020; Hu et al. 2020) by altering biogeochemical, ecological, and hydrological processes of the surface (Reynolds et al. 2005). According to the United Nations Convention to Combat Desertification (UNCCD 2015), 25% of the earth's land area has been degraded or is prone to degradation. The proportion of degraded lands is likely to increase to 30–40% of the total area in the future (Veron et al. 2006; Reynolds et al. 2007; Nkonya et al. 2016), which could affect approximately three billion people, particularly those living below the poverty line (Middleton and Thomas 1997; Hu et al. 2020).

Desertification has been a major concern for different regions of the earth, particularly the Mediterranean, Sahelian, African, and Chinese regions (Dregne 1986, 2002). Morocco is characterized by a Mediterranean bioclimate, where a large area is under the threat of desertification. Notably, this country's arid and semi-arid regions are the most ecologically sensitive areas. Actually, nearly 92% of the national territory is under the effect of this phenomenon (Ghanam 2003; Hammouzaki 2013; Lamqadem et al. 2018). A combination of climatic (irregular precipitation and increased frequency of periods of drought) and anthropogenic processes (overexploitation of the environment, continuous overgrazing, destruction of vegetation areas) contributes to desertification (Darouiche et al. 2015; Benmohammadi et al. 2001; Benbrahim et al. 2004; Houlidi et al. 2004; SEGHIR et al. 2019).

Aware of the extent of the phenomenon, several researchers have been interested in studying the phenomenon of desertification at the level of Morocco (Ghanam 2003; Benbrahim et al. 2004; Mahyou et al. 2010; Sinsin 2018) as well as at the level of several regions concerned by this problem, in particular, the basin of the high Ouergha—Central Rif (Ech-Chahdi et al. 2022), the basin of Guercif—Eastern Morocco (Bengrich 1988), the basin of the Moulouya (Mokhtari 2016), the plain of Tafrata—Central Eastern Morocco (SEGHIR et al. 2019), the Souss basin (Bouabid et al. 2010), the watershed Oued El Maleh (Lahlaoi et al. 2017). However, our studied basin has never been the subject of similar studies despite the fact that it suffers from high levels of desertification. Our choice to lift the veil on

the situation of desertification in the region is backed up by the need to raise the attention of decision-makers and serve as basis for adequate management actions.

Monitoring the spatiotemporal pattern of desertification is essential to limit the adverse effects of this hazard (Meng et al. 2007; Guang et al. 2017). Several methods exist to investigate the desertification process. The methods include direct observation (Collado et al. 2002; Lam et al. 2010), the use of mathematical algorithm (Afrasinei et al. 2017, 2018), and remote sensing technologies (Huang and Cai 2009; Li et al. 2013; Xue et al. 2013). Over the last three decades, the remote sensing-based approach has been emerging as an effective means to monitor spatiotemporal patterns of desertification (Huang and Siegert 2006; Pan and Li 2013). Remote sensing, in combination with a geographic information system (GIS), is a cost-effective approach that enables a quick assessment of various land features in space and time due to the availability of high-resolution multitemporal satellite images (Hostert et al. 2001; Helldén and Tottrup 2008; Wang et al. 2012).

The existing studies offer a range of remote sensing-based techniques for monitoring desertification, such as spectral mixture analysis (Collado et al. 2002; Huete et al. 2003; Khiry 2007; Pu et al. 2008; Sun et al. 2017), bi-temporal change (Pannenbecker 2006), image transformation, such as TCT (Louis et al. 2016; Zanchetta et al. 2016) and spectral index (Xiaodong et al. 2013; Lamchin et al. 2016; Feng et al. 2018). Various index-based approaches are widely used to investigate the degradation of various land features (Zhao et al. 2013). For instance, Normalized Difference Vegetation Index (NDVI) and Modified Soil Adjusted Vegetation Index (MSAVI) are commonly used to monitor the conditions of vegetation while assessing desertification (Linli et al. 2006; Xu et al. 2009; Yu et al. 2013; Ren et al. 2014; Wu et al. 2019). Indices such as albedo and the Topsoil Grain Size Index (TGSI) can detect spatial heterogeneity of soil texture (Xiao et al. 2006; Liu et al. 2018a). Indeed, many researchers worldwide have successfully used these indices for desertification assessment (Ma et al. 2011; Mfondoum et al. 2016; Vorovencii 2017; Jiang and Lin 2018; Liu et al. 2018b; Wei et al. 2018).

Zeng et al. (2006) proposed the albedo–NDVI feature space model to analyze desertification in a 2D feature space. For their part, Feng et al. (2018) developed another feature space model albedo–MSAVI. Other authors have used feature space based on albedo–TGSI (Guo et al. 2020; Wei et al. 2020). Nevertheless, the NDVI–albedo model is the most widely used by researchers. Nevertheless, the NDVI–albedo model is the most used by researchers thanks to its relevance and efficiency for the quantitative assessment of desertification in several regions of the world. Indeed, the NDVI and the albedo present a robust negative correlation reflecting the state of desertification.

The application of different approaches is context dependent. Our study will be based on the method of spectral indices, which makes it possible to extract many indices (TGSI, albedo, NDVI and MSAVI). Several combinations of these indices will be tested thanks to the correlation. The best combinations will be used to construct the corresponding feature spaces. The precision will be evaluated to determine the study area's most suitable model. The latter has never been studied in desertification despite all the

apparent signs showing that it suffers from the phenomenon (silting, erosion, degradation of the plant cover, soil salinization, etc.).

This study has set the following objectives: 1—map the different classes of desertification in the Middle Moulouya basin in 2018 using Sentinel-2 imagery which has the best resolution (10 m). 2—integrate indicators derived from remote sensing data to detect areas affected by desertification in 2018 and assess local processes. 3—make a correlation of the different biophysical indices (NDVI, albedo, MSAVI and TGSI) and a linear regression for the strongly correlated indices.

2 Materials and methods

2.1 Study area

This study focused on the Middle Moulouya basin, located in the Center East of Morocco (Fig. 1) between latitudes 32°50'–33°50' North and longitude 4° West. The basin has a total area of 14,355 km2, with an altitude varying from 534 to 3321 m (Mountain Bounacer). The High Plateaus limit this zone to the East, the Middle Atlas pleated to the West, the High Atlas to the South, and the threshold of Bouyacoubat to the North. The area is adjacent to three regions: Fez-Meknes, Oriental, and Daraa Tafilalt.

Due to its geographical position, the basin is characterized by an arid to semi-arid climate with hot summers and cold-dry winters. The region receives varying mean annual precipitation ranging from 160 to 300 mm. Temperatures also significantly vary from a maximum of 45 °C in summer to -2 °C in winter. The basin also has a very high potential for evapotranspiration (Kaemmerer et al. 1990; HassaniM et al. 2013; Saadi et al. 2021).

The study area is crossed by the river Moulouya which drains the waters towards the Mediterranean. Two species of natural vegetation are prevalent: Alfa (Stipa tenacissima) (over 80%) and Wormwood (Artemisia Herba-Alba) (Tag 2003). However, the locals overexploited such vegetation cover as part of pastoral activities. Agropastoralism is the major source of livelihood in the study area.
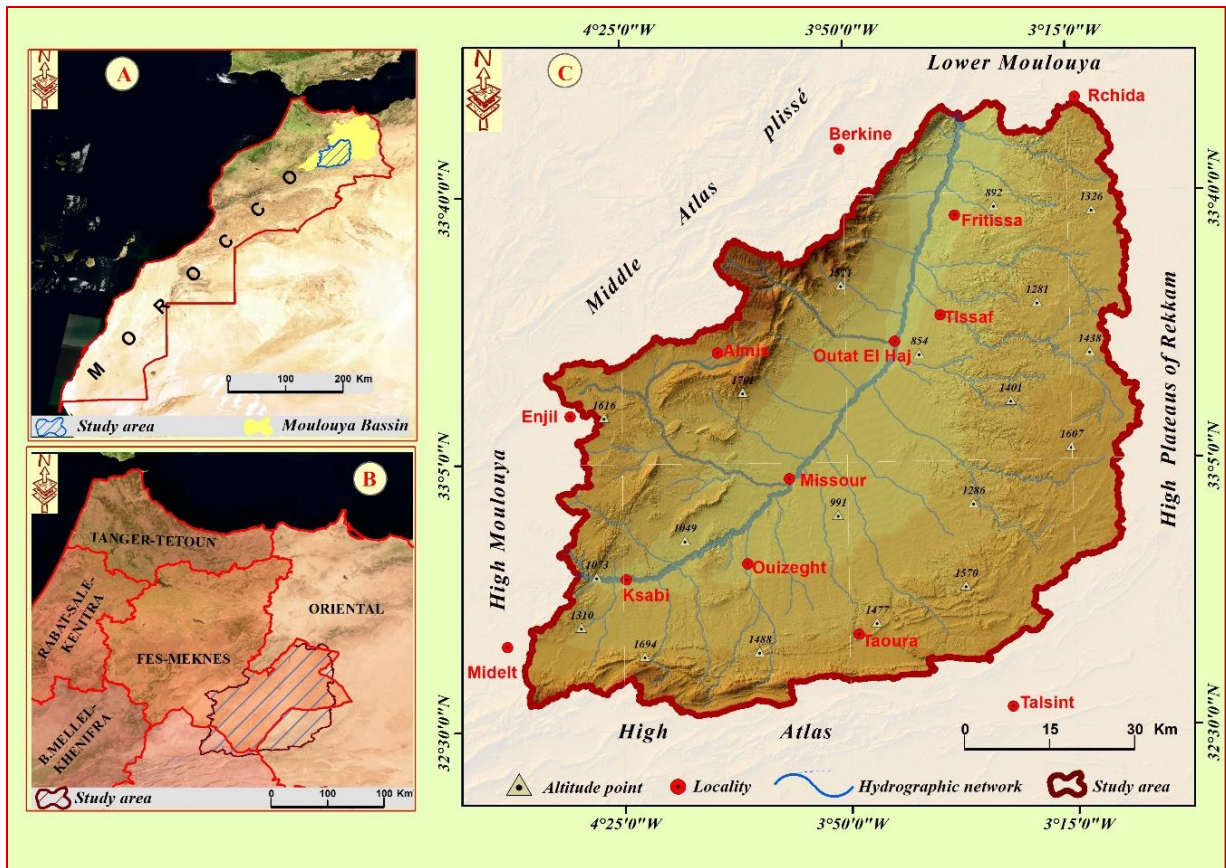
Fig. 1 Geographical location of the Middle Moulouya Basin **A** Location relative to the map of Morocco, **B** Location of the basin relative to the map of the administrative division of the regions and **C** map of the basin

2.2 Data

In this work, the evaluation of the degrees of desertification in the basin of the Middle Moulouya was carried out using six images, which cover the whole basin, produced by the Sentinel-2 satellite, which was chosen because of the high temporal, spectral and spatial resolution of the images captured which will allow getting good results reflecting the truth of the ground. The Sentinel-2 multispectral images are composed of 13 spectral bands at different spatial resolutions of 10 m (4 bands), 20 m (6 bands) and 60 m (3 bands). These 13 bands cover a wide range of wavelengths from 440 to 2200 nm.

To realize the present work, we used the bands of the red and the infrared, blue, green, SWIR-1 and SWIR-2.

Satellite images of June 2018 were used, when the cloud cover was low (less than 10%). Besides, June images enable separating agricultural lands with natural vegetation as crops are usually harvested before that month. These multispectral images were obtained from https://scihub.copernicus.eu. Table 1 presents the characteristics of Sentinel-2 satellite images.

Table 1 Characteristics of Sentinel-2 satellite imagery used in this study

Bands	Spatial resolution (m)	Wavelength (μm)
B 01: Aerosols	60 m	0.443
B 02: Blue		0.490
B 03: Green	10 m	0.560
B 04: Red		0.665
B 05: Near infrared 2		0.705
B 06: Near infrared 3	20 m	0.740
B 07: Near infrared 4		0.783
B 08: Near infrared 1	10 m	0.842
B 08A: Near infrared 5	20 m	0.865
B 09: Atmosphere		0.945
B 10: Cirrus	60 m	1.375
B11: Medium infrared 1		1.610
B12: Medium infrared 2	20 m	2.190

2.3 Analytical approaches

The methodology adopted in this study was based on the extraction of various spectral indices such as NDVI, albedo, TGSI and MASVI that allowed to assess and monitor desertification. An overview of the methodology is shown in Fig. 2. It includes the following steps:

- Acquisition of Sentinel-2 satellite images;
- Data pre-processing (geometric correction, radiometric correction, etc.);
- Calculation of spectral indices (NDVI, albedo, TGSI and MSAVI);
- Analysis of the linear correlation between the spectral indices (NDVI–albedo, MSAVI–albedo, albedo–TGSI and TGSI–MSAVI) to choose the best correlated indices;
- Calculation of a degree of desertification index (DDI) based on the results of the regression analysis;
- Verification and validation of the desertification sensitivity map with Feld data.
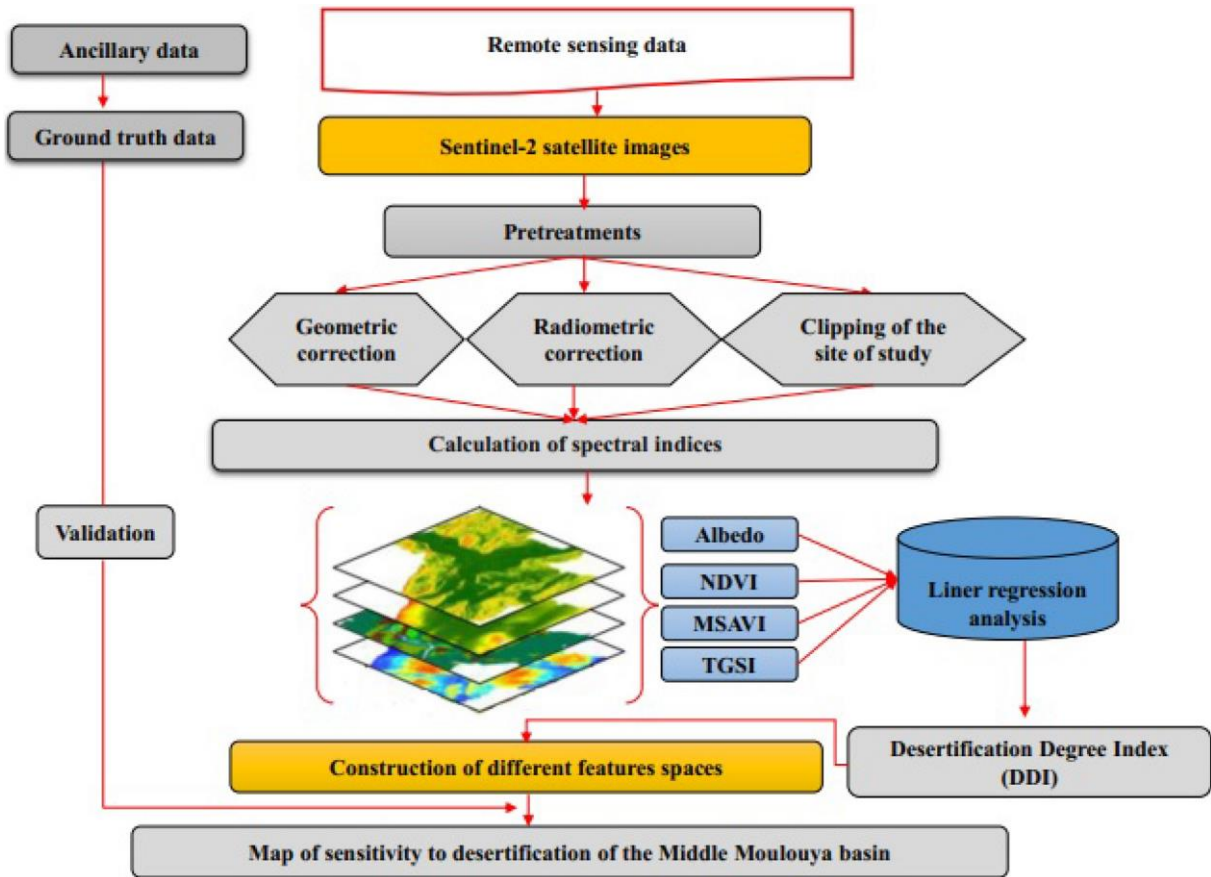
Fig. 2 Methodological flowchart

2.3.1 Preprocessing of satellite images

Before estimating values of various indices, this study carried out radiometric, atmospheric, and geometric corrections of the obtained satellite images. The radiometric correction aimed to eliminate all kinds of distortions in the images caused by the sensor, while the atmospheric correction removed the error caused by atmospheric radiation. To conduct radiometric calibration, digital number (DN) on the images were converted into radiance units first and then into Top of Atmosphere (TOA) surface reflectance units. This operation was performed using the Fast Line-Atmospheric Analysis of Hypercubes (FLAASH) tools based on a MODTRAN radiative transfer model integrated into the ENVI 5.3 software (Dao and Liou 2015).

The geometric correction was performed for all these images by selecting ground control points from topographic maps at 1/100.000, covering the study area: Immouzer of Marmoucha, Berkine, Debdou, Missour, Hassi and Ahmar, Midelt, Ksabi, Tameslent and Talsint. These maps were used for georeferencing satellite images concerning the conformal conical projected coordinate system of Lambert Nord-Morocco.

A total of six scenes were used to create mosaic imagery and then clipped to the boundaries of the study area as the final step in the pre-processing sequence.

2.3.2 Estimating different indices to evaluate desertification

Using the processed Sentinel-2 images, this study estimated values of four indices: NDVI, surface albedo, MSAVI and TGSI.

- **Normalized Difference Vegetation Index (NDVI)**

The Normalized Difference Vegetation Index (NDVI) is a dimensionless radiometric measure. NDVI has been widely used to investigate desertification in arid and semi-arid areas due to its extreme sensitivity to the presence, density, and state of the health of vegetation (Qi et al. 1994; Li and Liu 2003; Badreldin et al. 2014; Zhao et al. 2014; Lamchin et al. 2016; Lamqadem et al. 2018). The index incorporates the near infrared and red bands of satellite images using the following equation (Eq. 1) (Carlson and Ripley 1997):

$$NDVI = \frac{NIR - RED}{NIR + RED} \tag{1}$$

where RED and NIR are the red and near infrared bands of the Sentinel-2 image, respectively.

- **Surface Albedo:**

The albedo of land surface determines the radiant energy balance on the ground, indicating the extent of energy absorbed by the underlying surface (Liang 2001). It also shows the rate of solar radiation reflected by the surface in the shortwave spectral range (Ma et al. 2011). The values of albedo can be affected by soil moisture, vegetation cover, snow cover, and other soil surface conditions. An increased value of surface albedo could exhibit the evidence of desertification (Robinove et al. 1981; Xiao et al. 2006; Wang and Yan 2017). Albedo is inversely associated with NDVI. albedo was estimated using the following equation (Eq. 2) (Liang et al. 2003):

$$Albedo = \frac{[(0.35 * BLUE) + (0.13 * RED) + (0.373 * NIR) + (0.085 * SWIR\,1) + (0.072 * SWIR\,2) - 0.018]}{1.016} \tag{2}$$

where BLUE, RED, NIR, SWIR-1 and SWIR-2 are the bands of blue, red, medium infrared, near infrared 1 and near infrared 2 in the Sentinel-2 image, respectively.

Several researchers have used this basic equation designed for Landsat images for Sentinel-2 data (Kyalo 2017; Naegeli et al. 2017; Lamqadem et al. 2018; Guo et al. 2022).

- **Modified Soil Adjusted Vegetation Index (MSAVI):**

Although NDVI effectively assesses vegetation conditions, the index has inherent limitations in detecting sparsely vegetated areas where the influence of soil background is important. To address such an issue, this study utilized MSAVI to minimize the external effects and enhance the vegetation signal (Qi et al. 1994). The MSAVI is usually used in areas where the NDVI does not reflect the true state of

the vegetation, either due to lack of chlorophyll or low vegetation present in situ. It provides information on the state of the vegetation in these areas while separating the effects of the ground. Several studies showed that a lower MSAVI means sparser vegetation that indicates the presence of desertification (Li et al. 2016). The MSAVI was estimated using the following equation (Eq. 3) (Qi et al. 1994):

$$MSAVI = \frac{2 \times NIR + 1 - \sqrt{(2 \times NIR + 1)^2 - 8(NIR - RED)}}{2} \tag{3}$$

where RED and NIR are the red and near infrared bands of the Sentinel-2 images, respectively.

- **Topsoil Grain Size Index (TGSI):**

To detect areas with low vegetation and bare lands, this study estimated values of an index associated with soil texture, i.e., TGSI (Wang et al. 2002). The coarser grain size indicates a greater probability of desertification. The TGSI is based on both field spectral reflectance measurements and physical laboratory analyzes of the grain composition of the soil surface layer (Xiao et al. 2006). A negative TGSI value indicates vegetation or water bodies, while positive values correspond to a coarse soil. The higher the TGSI, the rougher the ground surface. The TGSI was estimated using the following equation (Eq. 4):

$$TGSI = \frac{RED - BLUE}{RED + BLUE + GREEN} \tag{4}$$

where RED, BLUE and GREEN are the red, blue, and green bands of Sentinel-2 satellite images, respectively.

2.3.3 Normalization of spectral indices

The estimated values of various spectral indices were normalized to eliminate the dimensional differences between the different indices used. The normalization process was carried out using the Eqs. 5, 6, 7 and 8, listed in Table 2.

Table 2 Normalization equation for spectral indices

Spectral indices	Equation of normalization	Equation no.
Albedo	$A = \frac{(Albedo - Albedo_{min})}{(Albedo_{max} - Albedo_{min})} \times 100$	(5)
MSAVI	$M = \frac{(MSAVI - MSAVI_{min})}{(MSAVI_{max} - MSAVI_{min})} \times 100$	(6)
TGSI	$T = \frac{(TGSI - TGSI_{min})}{(TGSI_{max} - TGSI_{min})} \times 100$	(7)
NDVI	$N = \frac{(NDVI - NDVI_{min})}{(NDVI_{max} - NDVI_{min})} \times 100$	(8)

2.3.4 Extraction of the different degrees of desertification in the basin Middle Moulouya

The extraction of the different degrees of desertification is based on the analysis of several pair combinations of spectral indices to choose the one that best discriminates against the other classes of desertification. These indices were extracted for 345 randomly selected points throughout the study area using a regular grid where the points were spaced 3000 m apart. We extracted the pixel values for each point corresponding to each chosen index (NDVI, albedo, TGSI and MSAVI).

We have chosen to test four combinations, namely: Albedo–NDVI, albedo–MSAVI, albedo–TGSI and TGSI–MSAVI, to take the best correlated combination to build the characteristic space which will make it possible to extract the index degree of desertification and, thus, produce the desertification map of the study region.

Linear regression analysis is based on the following equation (Eq. 9):

$$\mathbf{Y} = \mathbf{a} + \mathbf{b}\mathbf{x} \tag{9}$$

where $\mathbf{x}$ represents an independent variable; $\mathbf{y}$ represents a dependent variable; $\mathbf{a}$ is the point of intersection of the regression line and the y axis; $\mathbf{b}$ is the slope of the regression line.

The statistical regression analysis of the four feature space indices was then carried out using SPSS software, which made it possible to study the quantitative relationships between these different chosen indices. We will construct the feature space model from the pair of indices whose correlation is the most significant. This model will be used to draw up a map of degrees of desertification in the study area.

2.4 Construction of the desertification degree index (DDI)

The Index of Degree of Desertification (DDI) is a model used by researchers to map the sensitivity to desertification, with precision, at the level of arid to semi-arid (Ma et al. 2011; Pan and Li 2013; Becerril-Piña et al. 2016). The IDD is based on the spatial classification of constructed feature space.

According to the research results of Verstraete and Pinty (1996), different desertification zones can be effectively distinguished by dividing the albedo–NDVI feature space in the vertical direction which represents the desertification trend. The equation (Eq. 10) for the degree of desertification index is as follows:

$$DDI = K \times NDVI - Albedo \tag{10}$$

where "IDD" is the index of degree of desertification for the two feature space models and K is determined by the slope of the fitted straight line in the feature space.

The calculated values of the degree of desertification are then classified into five categories using the Jenks natural break algorithm (Jenks 1963; Ma et al. 2011). These five categories of desertification are as follows: extreme desertification, high desertification, moderate desertification, low desertification and no desertification.

The classification of degrees of desertification is based on the method of natural breaks which consists of the natural grouping of data. Its limit is set at the position where the data values are relatively different.

2.4.1 Accuracy assessment

To verify and evaluate the accuracy of the desertification map, we selected 160 points that were the most representative of all the desertification classes obtained. 60 of these verification points were taken in the field using a GPS. The other 100 verification points were extracted from high-resolution remote sensing images. These images are uniformly selected and interpreted based on Google Earth data and Sentinel-2 true color images.

The verification points were chosen to cover all degrees of desertification: extreme, severe, moderate, low and no desertification. Finally, the confusion matrix was constructed to have the classification accuracy of the producer, the user, and the accuracy of the overall classification, as well as the Kappa coefficient. The result of the accuracy calculation was used for the validation of the desertification map.

3 Results
3.1 NDVI, Albedo, MSAVI and TGSI

Figure 3 represents the calculation results of the four spectral indices (NDVI, albedo, TGSI and MSAVI). NDVI values range from -0.16 to 0.74 (Fig. 3a). The low values of NDVI correspond to the denuded areas with desert behavior which are generally found on the borders of the Moulouya river. In contrast, the high values reflect soils with high vegetation cover corresponding to the forests in the Middle Atlas Plissé and the High Atlas, as well as the irrigated lands along the Moulouya river.

Surface albedo values vary between 0.03 and 0.89 (Fig. 3b). The results obtained by this indicator are consistent with the results obtained by the Normalized Vegetation Index (NDVI). Indeed, the low values of the albedo representing a dense vegetation cover are also located at the level of the Middle Atlas Plissé and the High Atlas Mountains as well as at the edges of river Moulouya. As for the high values of the albedo, they reflect areas with low vegetation, such as steppe areas. The TGSI index provides information on the topsoil grain size. The values of this index vary between 0 and 0.92 (Fig. 3c). The highest values indicate a coarse grain size of the topsoil and, thus, a high sand content and consequently more degraded areas located mainly at the level of the center of the Middle Moulouya basin. The MSAVI index values range from -0.10 to 0.65 (Fig. 3d). Low values represent water and bare soil, while high values correspond to dense vegetation.

As the study area comprises several landscape units (forests, steppe rangelands), we resorted to the use of different spectral indices that better fit the type of landscape unit. Indeed, the MSAVI gave better results in areas where vegetation is sparse, while the NDVI presented these areas as bare, especially in the center of the basin.

The albedo index highlighted areas with bare soil, while the TGSI index focused on areas with coarse soil where desertification is advanced, as is the case along the Moulouya river.
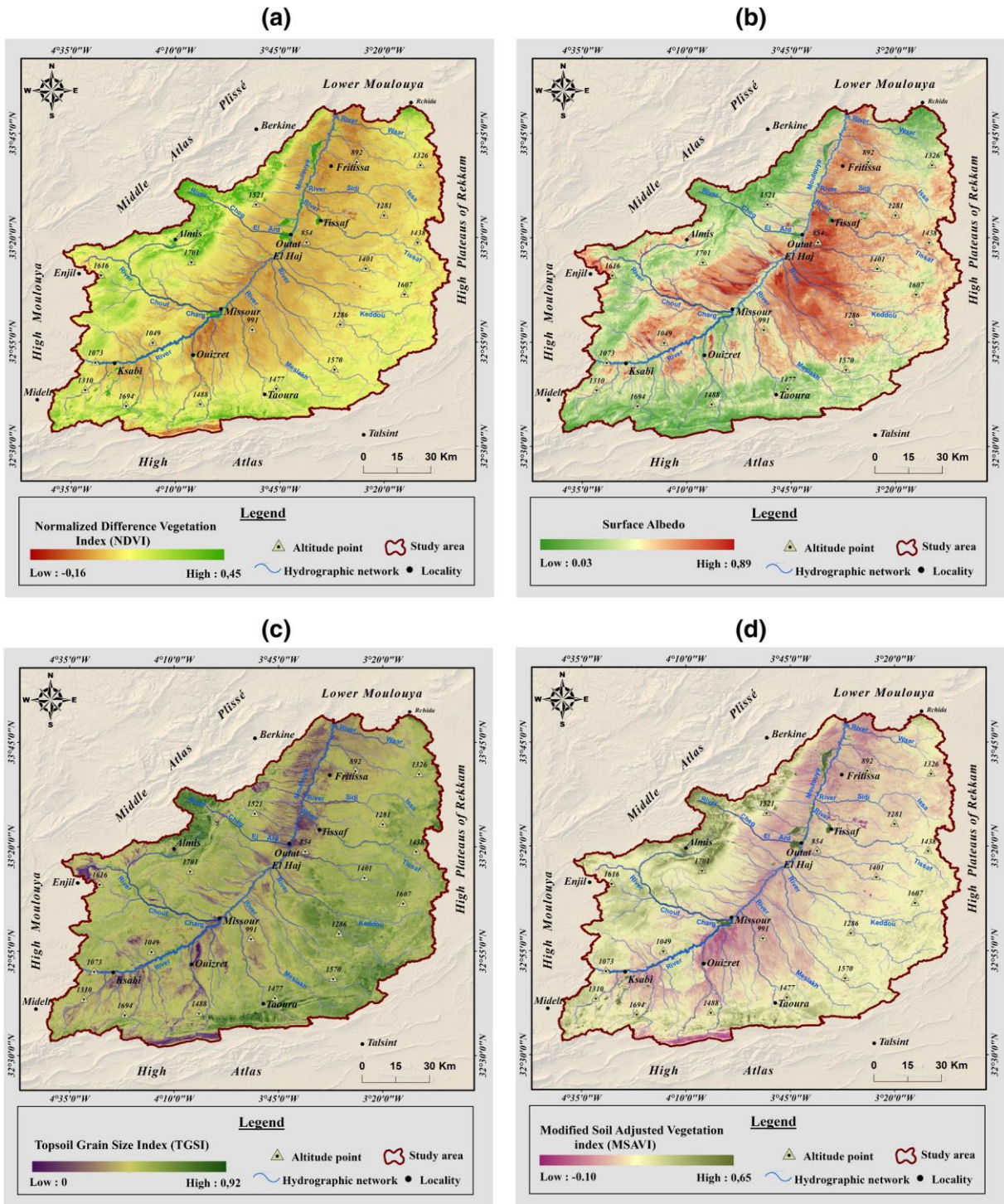
Fig. 3 The four spectral indices derived from (a) NDVI; (b) Albedo; (c) TGSI; (d) MSAVI.

3.2 Construction of the different features spaces

A feature space image is a plot of the data file values of one band against another (essentially a scatter plot with one point for each pixel in the image). The position of the pixels in the feature space image is defined by the spectral values of the two selected bands.

From the four surface indices chosen previously, we performed four combinations to construct the corresponding features spaces, using the 2D scatterplot tool of the ENVI 5.3 software. These combinations are as follows: albedo–NDVI, albedo–TGSI, albedo–MSAVI and TGSI–MSAVI. Figure 4 groups together the four feature spaces constructed.
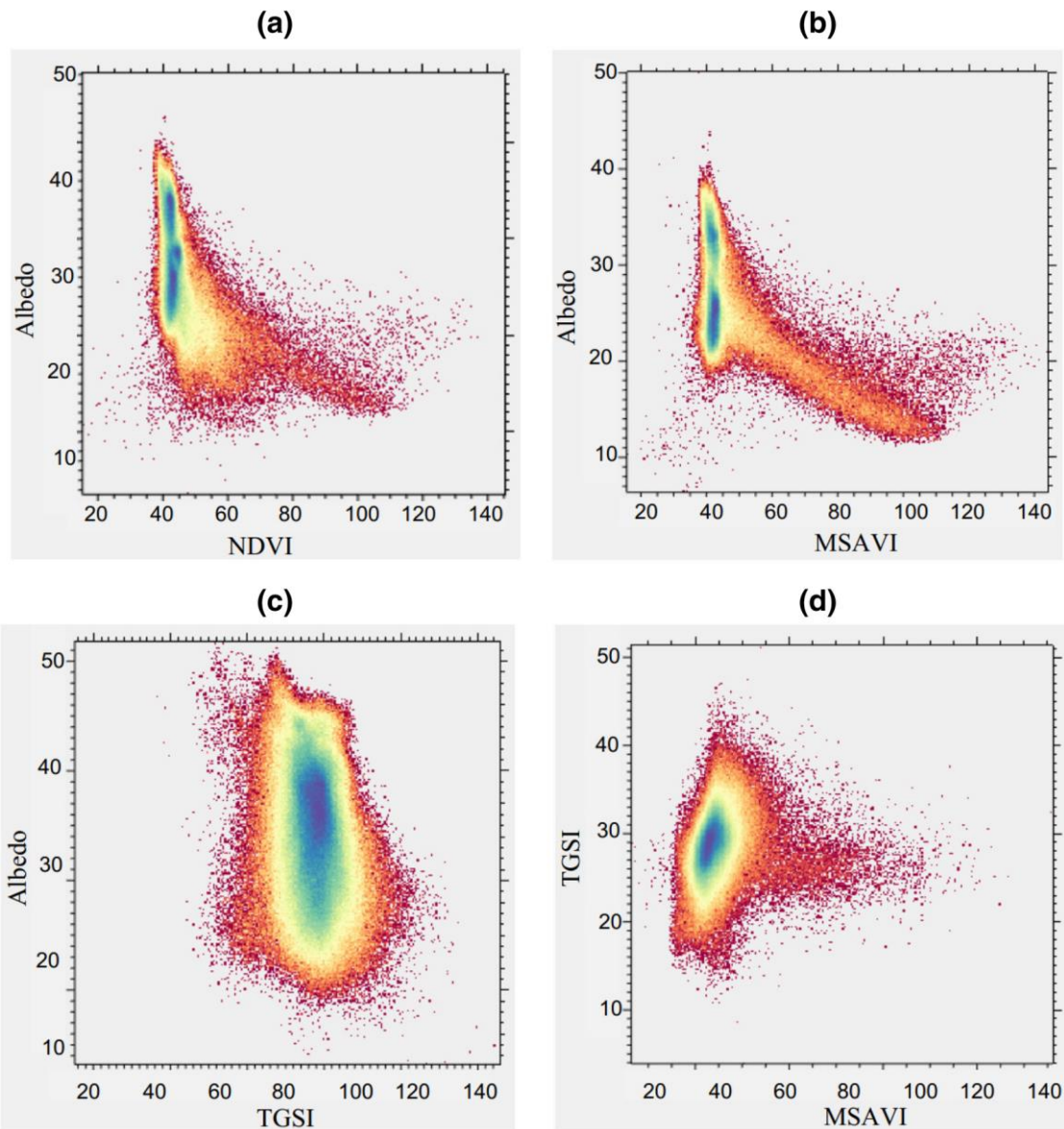
Fig. 4 The different characteristic spaces constructed: (a) NDVI-Albedo; (b) Albedo-MSAVI; (c) Albedo-TGSI; (d) TGSI-MSAVI

The feature space image is represented as a raster image and has a color associated with each pixel. The colors (or grayscale intensity) represent the cumulative frequency, i.e., the number of pixels in the original image that have the given (x, y) combination.

We, thus, constructed four feature spaces using typical desertification indices to reflect the interaction effect between these indices. Thus, areas where desertification is at an advanced stage, surface vegetation cover decreases (with low values of NDVI and MSAVI) and exposed soil surfaces increase (with high values of TGSI and albedo). These different feature spaces will be compared to choose the one best suited to our study area.

Indeed, the choice of the most suitable model for our region will be based on the results of the significant linear correlation.

3.3 Calculation and analysis of the linear regression between the indices of the feature space

Four combinations of typical desertification indices were tested. In three of these combinations, we chose albedo as the dependent variable and NDVI, TGSI and MSAVI as independent variables. For the fourth combination, TGSI is the dependent variable and MSAVI is the independent variable.

The linear regression equations between the two surface parameters constituting each feature space, along with the correlation and determination coefficients are presented in Fig. 5. Significant negative correlations were observed between albedo and MSAVI ($r = -0.76$) and between albedo and NDVI ($r = -0.76$) (Fig. 5a, b). This indicates that albedo decreases when NDVI and MSAVI increase, indicating little to no desertification and vice versa. When they decrease, albedo increases showing that the area is affected by desertification. While albedo and TGSI as well as MSAVI–TGSI show a weak correlation with respective correlation coefficients of ($r = -0.43$) and ($r = 0.39$) (Fig. 5c, d).

From the results obtained from the linear regression analysis, the feature space models selected are albedo–NDVI since it explains 54% of the observed variability ($R2 = 0.54$) and the MSAVI–albedo which explains 59% of the observed variability ($R2 = 0.59$). Therefore, they will allow us to make predictions for desertification and extract the degrees of desertification.
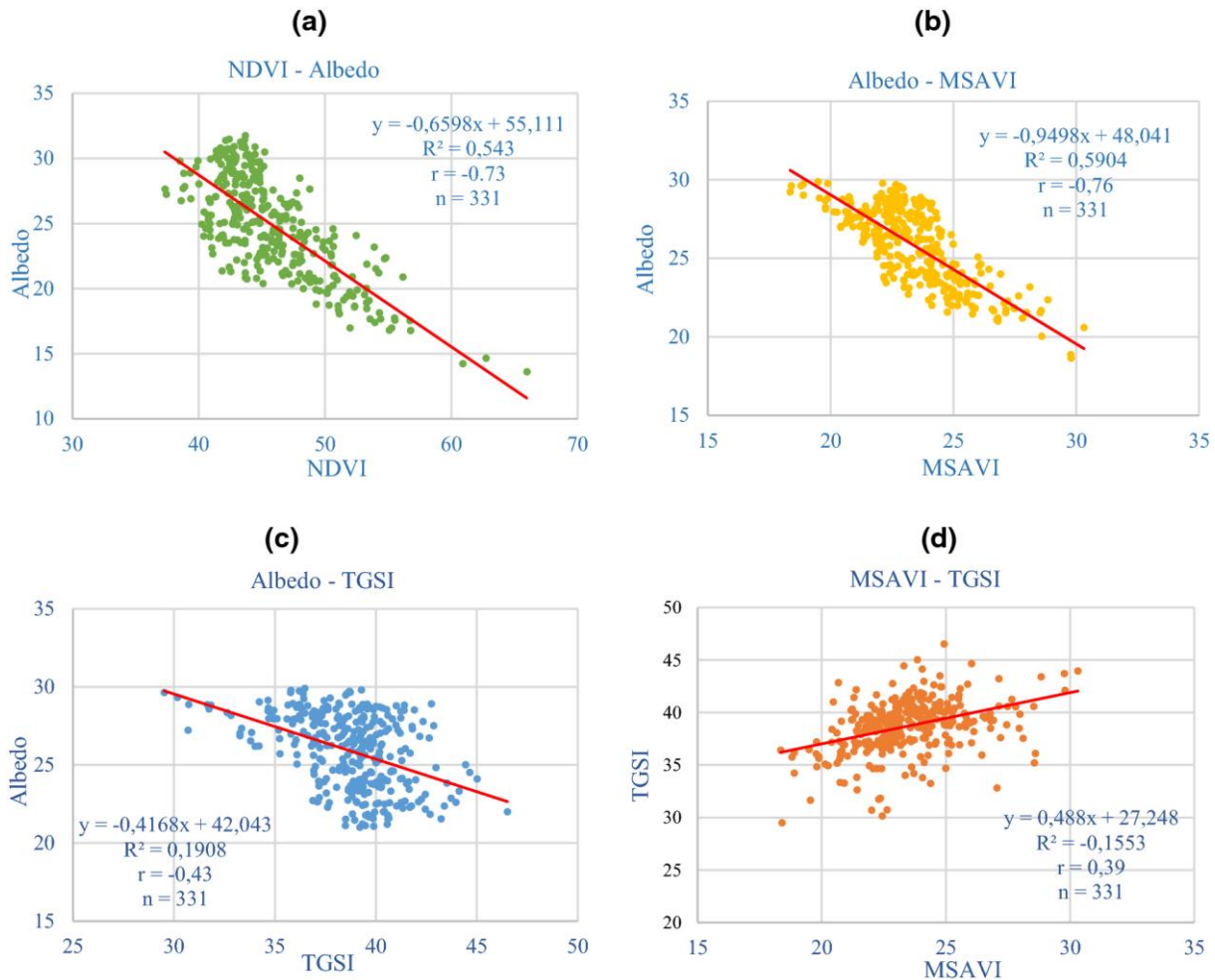
(a) NDVI - Albedo

y = -0,6598x + 55,111
R² = 0,543
r = -0.73
n = 331

(b) Albedo - MSAVI

y = -0,9498x + 48,041
R² = 0,5904
r = -0,76
n = 331

(c) Albedo - TGSI

y = -0,4168x + 42,043
R² = 0,1908
r = -0,43
n = 331

(d) MSAVI - TGSI

y = 0,488x + 27,248
R² = -0,1553
r = 0,39
n = 331

Fig. 5 Correlation analysis between the variables of the different features spaces: (a) NDVI- Albedo; (b) Albedo-MSAVI; (c) Albedo-TGSI; (d) TGSI-MSAVI

3.4 Principle of construction of a monitoring model based on the feature space: case of the NDVI-Albedo feature space

Several studies have demonstrated the effectiveness of using the albedo–NDVI feature space to distinguish between different classes of desertification. Indeed, areas with high albedo and low NDVI show low vegetation cover and Reduced surface roughness. Consequently, these areas are affected by severe desertification, contrary to areas with low Albedo and high NDVI. To construct the albedo–NDVI scatterplot (Fig. 6b) and the albedo–NDVI feature space (Fig. 6a), we based ourselves on the values of the NDVI and the albedo previously extracted. We assumed a trapezoidal shape of the feature space by taking the albedo as the ordinate and the NDVI as the abscissa, as shown in the figure below (Fig. 6).

This figure shows the different areas of desertification. A, B, C and D represent four extreme states. Indeed, point A represents a dry soil devoid of vegetation (low NDVI, high albedo), point B represents a soil with high vegetation and low moisture (high NDVI, high albedo), point C indicates soil water abundance with high vegetation cover (high NDVI, low albedo) and point D indicates bare soil with water abundance (low NDVI, low albedo). The upper boundary (AB) represents the high albedo line, it

reflects lands affected by drought and aridity with low vegetation cover (Albalawi and Kumar 2013). The lower boundary (CD) represents the low albedo line, which corresponds to wetlands.

The ABCD area contains all types of ground objects with a specific spatial differentiation rule.
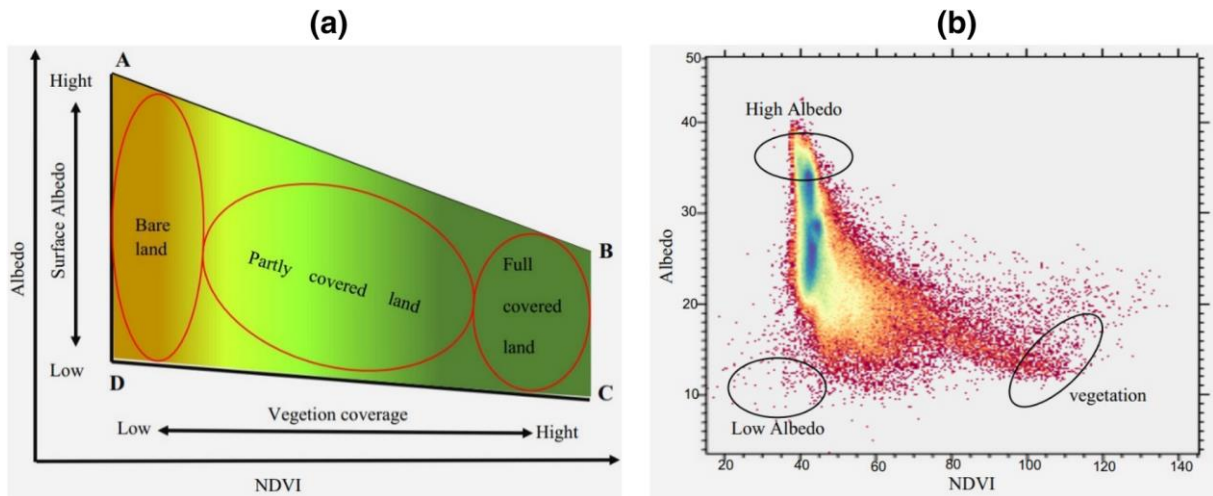

Fig. 6 (a) feature space of Albedo-NDVI; (b) Scatter plot of the Albedo-NDVI.

3.5 Results and comparison of the desertification degree index (DDI)

The Desertification Degree Index (DDI) is a model used by researchers to map desertification susceptibility accurately in arid to semi-arid areas (Ma et al. 2011; Pan and Li 2013; Becerril-Piña et al. 2016). The IDD is based on the spatial classification of constructed feature spaces.

For our study, the construction of the characteristic models NDVI–albedo and MSAVI–albedo will allow us to extract the different degrees of desertification at the level of the Middle Moulouya basin.

According to Verstraete and Pinty (1996), different desertification zones can be effectively distinguished by dividing the two characteristic spaces albedo–NDVI and MSAVI–albedo in the vertical direction that represents the desertification trend as shown in the figure below (Fig. 7).
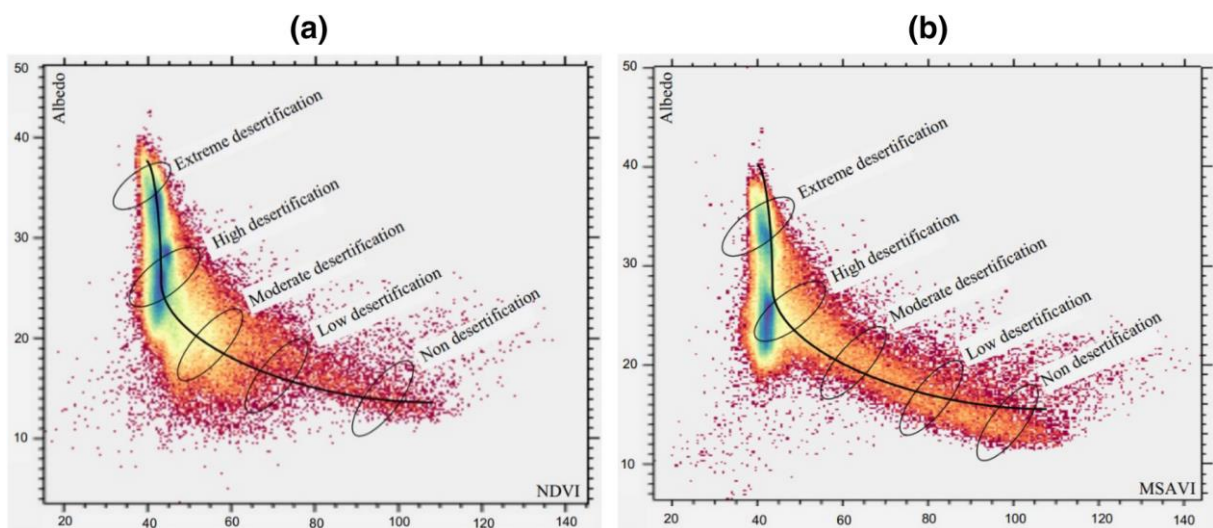

Fig. 7 (a) Different degrees of desertification in the Middle Moulouya basin: (a) NDVI-Albedo; (b) MSAVI-Albedo

Indeed, the closer one gets to point O (0, 0), the greater the desertification. The distance between the sets of extreme desertification points and the point O (0, 0) is the smallest, followed by the sets of severe, moderate, weak desertification points, and the distance between the sets of non-desertification points is the largest.

Based on the linear relationship, the region perpendicular to the albedo–MSAVI feature space and the albedo–NDVI feature space can be determined by a simple binary linear polynomial, as proposed by Pan and Li (2013). The DDI can be obtained, therefore, from the following equations (Eqs. 11 and 12):

where "DDI" is the index of degree of desertification for both feature space models, and K is determined by the slope of the fitted straight line in the feature space. The table below (Table 3) shows the value of K according to the model used.

Table 3 Statistical values of K for the two feature space models

Feature space models	K
Albedo–NDVI	1.51
Albedo–MSAVI	1.05

The calculated values of the degree of desertification are then classified into five categories using Jenks' natural break algorithm (Jenks 1963; Ma et al. 2011). Several researchers have successfully used this algorithm (Ma et al. 2011; Pan and Li 2013; Becerril-Piña et al. 2016) to classify the phenomenon of desertification in the drylands. It is a data clustering method designed to determine the best arrangement of values in different classes (Becerril-Piña et al. 2016). The variance within classes is reduced and the variance between classes is maximized (Jenks 1963).

Therefore, the five categories of desertification obtained by Jenks' classification are as follows: extreme desertification, high desertification, moderate desertification, low desertification and non-desertification. These different categories as well as the corresponding DDI values are represented in Table 4.

Table 4 Statistical analysis of the results of extraction of information on desertification by Albedo-NDVI, Albedo-MSAVI and Albedo-TGSI.

Classes de desertification	DDI of NDVI-albedo	DDI of MSAVI-albedo
Non-desertification	$DDI \geq 89.23$	$DDI \geq 30.77$
Low	$89.23 < DDI \leq 56.85$	$30.77 < DDI \leq 14.77$
Moderate	$56.85 < DDI \leq 43.20$	$14.77 < DDI \leq 7.07$
Severe	$43.20 < DDI \leq 32.38$	$7.07 < DDI \leq 0.78$
Extreme	$DDI \leq 32.38$	$DDI \leq 0.78$

3.6 Desertification mapping

After extracting the degrees of desertification using the DDI and Jenks classification, a mapping of the DDI distribution was performed for the two models (albedo–NDVI) and (albedo–MSAVI) as shown in Fig. 8.
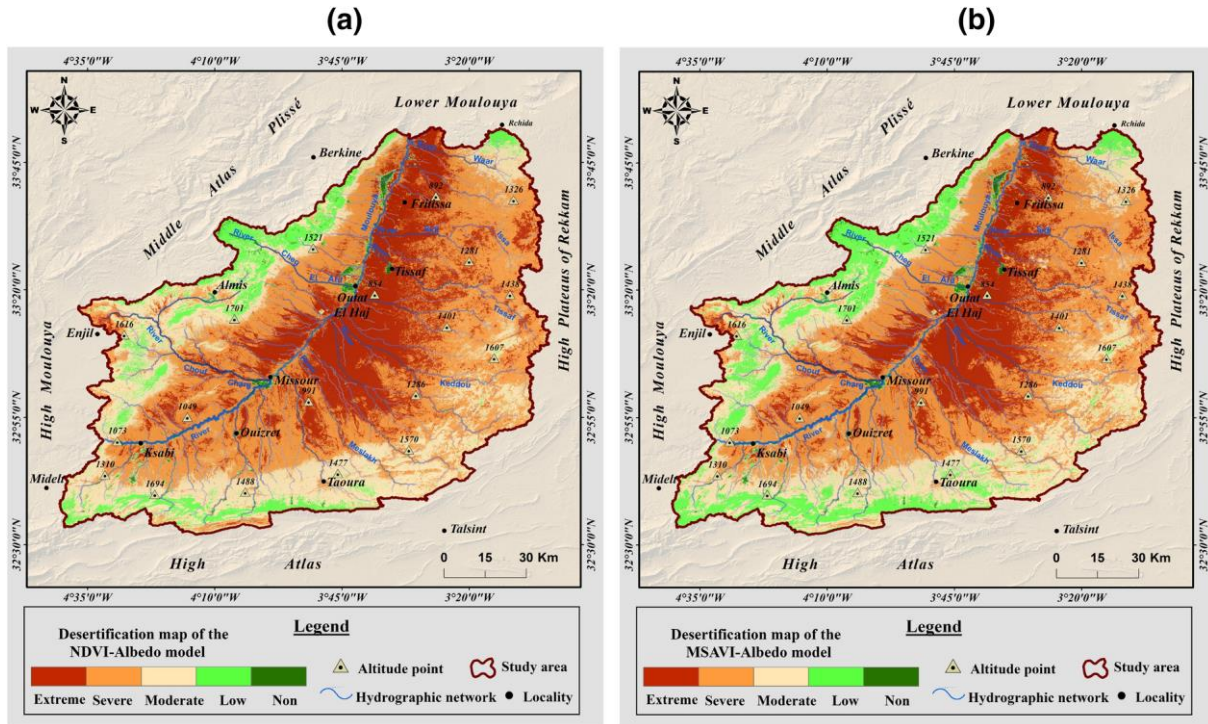

Fig. 8 Map of the state of desertification in the Middle Moulouya basin in 2018. (a) NDVI- Albedo; (b) MSAVI- Albedo.

The calculation results of the two models used: NDVI–albedo and MSAVI–albedo are shown in Table 5.

Table 5 Statistical analysis of the extraction of information on desertification by albedo–NDVI, albedo–MSAVI and albedo–TGSI

Desertification categories	NDVI-Albedo		MSAVI-Albedo	
	Area (Km^2)	Portions (%)	Area (Km^2)	Portions (%)
Non desertification	114,32	0,80	127,99	0,89
Low	1595,62	11,12	1758,77	12,25
Moderate	3522,74	24,54	3720,10	25,92
Severe	6087,07	42,40	5899,02	41,09
Extreme	3035,25	21,14	2849,12	19,85
Total	14355	100,00	14355	100,00

According to the results obtained by the NDVI–albedo model, 88.08% of the Middle Moulouya basin is affected by desertification, including 24.54% for moderate desertification, an area of 3522.74 km2, 42.40% for severe desertification is an area of 6087.07 km2 and 21.14% for extreme desertification is
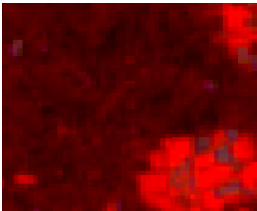
an area of 3035.25 km2. As for areas with low desertification and non-desertification, they, respectively, represent 11.12% or 1595.62 km2 and 0.8% or 114.32 km2 of the study area.

The MSAVI–albedo model, for its part, shows that 86.86% of the Middle Moulouya basin suffers from moderate to extreme desertification, of which 25.92% for moderate desertification, or 3720.10 km2, 41 0.09% for severe desertification, or 5899.02 km2 and 19.85% for extreme desertification, or 2849.12 km2. As for areas with low desertification and non-desertification, they, respectively, represent 12.25% or 1758.77 km2 and 0.89% or 127.99 km2 of the study area.

The two models gave an almost similar spatial distribution of desertification with a slight difference in the areas of each category (Fig. 8). The zones of extreme and severe desertification are the most common at the basin level. They are located mainly at the level of the center and the High plateaus of Rekkam. Moderate desertification affects the borders of the High Atlas and the Middle Atlas Plissé and part of the High plateaus of Rekkam. The low desertification is located in the irrigated areas along the Moulouya river, its tributaries, and the forests of the High Atlas and the Middle Atlas Plissé.

The different categories of desertification and the description of each category with their satellite images are summarized in Table 6.

Table 6 Summary and description table of the different categories of desertification

Class	Description	Image	Sentinel-2 image
Non desertification	Located at the borders of the river Moulouya and its tributaries and the forests of the Middle Atlas Plissé and the High Atlas. These zones are characterized by low degradation factors, and a good balance between socio-economic components and land use.		
Low	Make up most of the Middle Atlas Plissé and High Atlas. These areas require the application of good land management practices to maintain ecosystem balance.		
Moderate	Located at the borders of the Pleated Middle Atlas and the High Atlas as well as at the level of the Rekkam High Plateaus. Being very susceptible to desertification, they require intervention to maintain the balance between environment and anthropogenic activities.		

Severe	Located at the level of the center of the basin and the High Plateaus of Rekkam. The human-environment balance is completely broken and needs to be rebuilt again.		
Extreme	Located at the level of the center of the basin and the High Plateaus of Rekkam. It affects the entire basin at different scales and manifests poor management of the territory.		

3.7 Evaluation and comparison of the accuracy of the desertification map

As mentioned, we used 160 points surveyed with GPS to verify and validate the results with the field data. Indeed, the evaluation of the accuracy allows us to verify if the pixels of the satellite image, especially those corresponding to the verification points chosen in the field, correspond to the correct output class. To do this, we have constructed the confusion matrix of the two models selected, as shown in Tables 7 and 8. This matrix compares the classes obtained by classification with the reference points (160 points) by calculating specific indices such as the global accuracy index, the Kappa coefficient, the user's accuracy, and the producer's accuracy.

According to the results obtained, the overall accuracy reached 91.88% with a Kappa index of 0.89 for the NDVI–albedo model, and it reaches 93.75% with a Kappa index of 0.92 for the MSAVI–albedo model.

For NDVI–albedo, the use and production precisions of each class were 93.75% and 96.77% for non-desertification, 88.46% and 92% for low desertification, 90.91% and 88.24% for moderate desertification, 90.91% and 85.75% for severe desertification, 94.44% and 97.14% for extreme desertification.

As for the MSAVI–albedo model, the use and production precisions are superior to those of the NDVI–albedo model for all classes. Indeed, the precisions of use and production are of the order of 94.12% and 96.97% for non-desertification, 89.29% and 92.59% for low desertification, 89.29% and 90.63% for moderate desertification, 93.33% and 90.32% for severe desertification, 94.74% and 97.30% for extreme desertification. It can be seen that the two feature space models selected have a high overall classification accuracy, with equally high Kappa indices. Nevertheless, the overall accuracy, as well as the Kappa index of the MSAVI–albedo model, are slightly higher than the NDVI–albedo model.

Table 7 Confusion matrix of the desertification map of the NDVI-Albedo model

Desertification category	Ground Truth					Total	User Accuracy (%)
	Non desertification	Low	Moderate	Severe	Extreme		
Non desertification	**30**	2	0	0	0	32	93,75%
Low	1	**23**	2	0	0	26	88,46%
Moderate	0	0	**30**	3	0	33	90,91%
Severe	0	0	2	**30**	1	33	90,91%
Extreme	0	0	0	2	**34**	36	94,44%
Total	31	25	34	35	35	**160**	
Producer Accuracy (%)	96,77%	92,00%	88,24%	85,71%	97,14%		
Overall Accuracy				91,88%			
Kappa index				0,89			

Table 8 Confusion matrix of the desertification map of the MSAVI-Albedo model

Desertification category	Ground Truth					Total	User Accuracy (%)
	Non desertification	Low	Moderate	Severe	Extreme		
Non desertification	**32**	2	0	0	0	34	94,12%
Low	1	**25**	2	0	0	28	89,29%
Moderate	0	0	**29**	1	0	30	96,67%
Severe	0	0	1	**28**	1	30	93,33%
Extreme	0	0	0	2	**36**	38	94,74%
Total	33	27	32	31	37	**160**	
Producer Accuracy (%)	96,97%	92,59%	90,63%	90,32%	97,30%		
Overall Accuracy				93,75%			
Kappa index				0,92			

4 Discussions

This work aimed to establish a model that quantitatively assesses the degree of desertification in the Middle Moulouya basin. Several typical spectral indices namely NDVI, albedo, MSAVI and TGSI were used to construct different feature spaces (albedo–NDVI, albedo–MSAVI, albedo–TGSI and TGSI–MSAVI). The values of these indices were extracted from at high-resolution (10 m) Sentinel-2 satellite

images. The linear correlation established for the different combinations revealed that only the albedo–NDVI and albedo–MSAVI combinations are significantly correlated. Therefore, the other two combinations (albedo–TGSI and TGSI–MSAVI) had to be discarded.

The degree of desertification was then calculated for the two models retained, by linear adjustment of the vertical position in the two feature spaces, thus making it possible to establish the map of the degrees of desertification of the study area. The latter showed a spatial gradient of the desertification of the Middle Moulouya basin, which goes from the center to the extremities of the basin. Indeed, the center of the basin is marked, in its majority, by severe to extreme desertification. In contrast, the further away one goes, the moderate to low desertification (High Plateaus of Rekkam, Middle Atlas, and High Atlas).

In our study area, we do not have a reference to compare our results because no study on desertification has been conducted to date in the study area. That is why we resorted to comparing the results obtained with Google Earth's image at high resolution. This comparison perfectly coincides with this work's results and the field's reality.

The construction of several feature spaces was mandatory because a single feature space model can only illustrate the state of desertification with high precision in areas with similar characteristics.

Indeed, the albedo–NDVI feature space model gives more accurate results for areas with dense vegetation cover (the High and Middle Atlas Plissé) than areas with sparse vegetation (the High Plateaus of Rekkam and the center of the basin). Because at the level of this kind of zone, the NDVI is influenced by the bottom of the soil, thus implying the reduction of the precision of classification of zones with moderate desertification.

As for the albedo–MSAVI feature, space model is more accurate for areas with low vegetation cover because it eliminates the influence of the soil background. As our study area is characterized mainly by areas with low vegetation cover (the High Plateaus of Rekkam and the center of the basin), we have introduced this index for a more precise assessment of desertification.

A comparison between the two models NDVI–albedo and MSAVI–albedo, showed that the results of the two classifications were almost similar. However, the accuracy of the MSAVI–albedo model is slightly higher for all classes.

These results prove that the MSAVI–albedo model better detects the vegetation in our study area, which is generally characterized by a sparse vegetation cover, as it makes it possible to extract better information relating to non-desertification, low desertification, and moderate desertification. As a result, this model is the most suitable for monitoring information and quantitative assessment of desertification in the study basin and regions with similar characteristics (arid and semi-arid regions).

The spatial distribution of desertification observed in our study is similar to those of Mokhtari (2016), who conducted a study on the dynamics of desertification in the Moulouya basin. He noted that the areas most affected by the phenomenon of desertification are both in the High Plateaus of Rekkam and the valley of the Middle Moulouya (center of the basin).

Many studies have used the same models as in the present research work, notably Wei et al. (2018, 2020) and Wu et al. (2019) in Mongolia, Guo et al. (2020) in Naiman Banner (China) and Becerril-Piña et al. (2016) in Mexico.

All the regions where these models have been applied have similar characteristics to our area study, mainly in arid to semi-arid climate. Therefore, these models are reliable and give an accurate assessment of desertification, thus making their use in the Middle Moulouya basin of great relevance.

The state of desertification raised by this study can be explained by two types of driving forces: climatic and anthropogenic. The analysis constitutes a primordial step for understanding and the fight against this phenomenon.

The first driving force is related to climatic conditions. Indeed, aridity and drought are the main characteristics of the Middle Moulouya basin, where aridity is more accentuated in the areas closest to the Moulouya river or at low altitude, which confirms our results raising a desertification severe to extreme in these areas.

For the drought, the basin experienced a succession of several dry years (1982–1984, 1986–1988, 1992–1993, 1998–1999, 2004–2005, 2011–2012 and 2013–2014). Climate data analysis shows that the region is characterized by low, irregular, and variable rainfall over time. These precipitations hardly exceed 200 mm year^{-1} (Fig. 9). The basin is also characterized by high temperatures which can reach 45 °C in July and August.
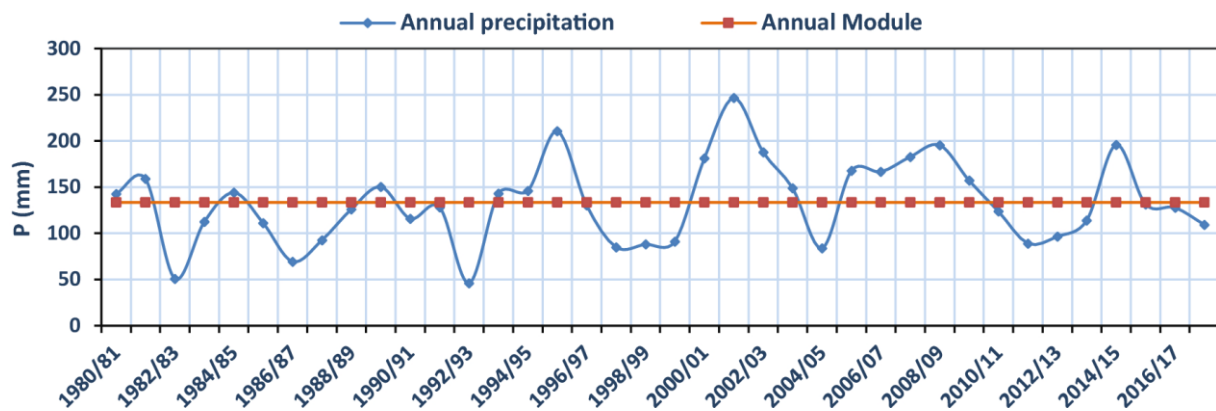

Fig. 9 variability of annual precipitation totals compared to the average of the Outat El Haj station for the period 1980-2017

These severe climatic conditions favor the appearance and evolution of the phenomenon of desertification, which is closely linked to the availability of water necessary for the growth of vegetation, which in turn protects the soil against water and wind erosion.

As for the second driving force, it is exercised by the anthropogenic activities of a population that continues to increase (Fig. 10). Indeed, the study area has experienced significant population growth, as its population increased from 203,529 inhabitants in 1994 to 233,856 in 2004, reaching 247,837 inhabitants in the last census of 2014 with a growth rate of 1.68%.
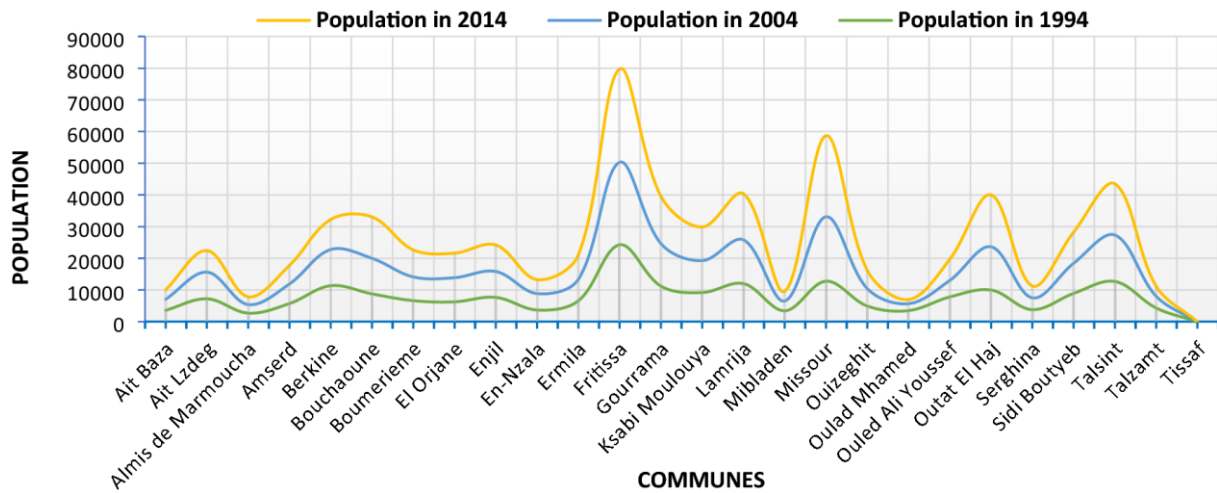
Fig. 10 Evolution of the population of the Middle Moulouya basin between 1994 and 2014 (Source: RGPH 1994, 2004 and 2014)

This rapid increase in population puts considerable pressure on natural resources. The overexploitation of these resources takes place in several forms, namely overgrazing and excessive cutting of woody plants in pastoral lands for domestic purposes. These activities modify land use by reducing and destroying the vegetation in these areas, thus exposing the soil to different types of degradation and the expansion of the phenomenon of desertification.

Moreover, human activity plays an important role in the salinity of soils in the region through anarchic practices related to agriculture and irrigation of land. This salinity leads to the loss of productivity of these lands (Fig. 11).

Fig. 11 Soil salinity problem in the Middle Moulouya basin

The combination of these two driving forces has led to the current state of desertification determined by this work. Indeed, the further one moves away from the center of the basin, the climatic conditions are better, and the population density is relatively low, which explains the classes of desertification of these areas, which range from low to moderate desertification.

This study has lifted the veil on the very advanced state of desertification on the scale of the Middle Moulouya basin, requiring rapid and immediate intervention to develop a program to combat this phenomenon and strategies for the rehabilitation of seriously affected areas.

5   Conclusions

Through this study, we proceeded to the construction of two models of feature spaces (NDVI–albedo and MSAVI–albedo) which were used for the quantitative characterization of desertification at the level of the Middle Moulouya basin. The results obtained using these models are much better than traditional methods based solely on vegetation cover indices, which have several limitations, especially in a low vegetation region. Of these two models, the MSAVI–albedo model can be the best suited to the study area consisting mainly of vast rangelands with sparse vegetation (High plateaus of Rekkam). At the same time, the NDVI–albedo model gives better results for areas with dense vegetation, such as the Middle Atlas and the High Atlas of our basin. However, these areas represent only a small portion of the territory studied. Given its effectiveness in monitoring desertification in our study area, the MSAVI–albedo model can serve as a reference for decision-makers working in national and regional natural heritage protection. This model can also be applied to other areas with the same surface characteristics. Based on the results of this work, an action plan should be put in place urgently to overcome the advanced situation of desertification in 2018 in the basin and limit land degradation. This work opens the opportunity in front for works in progress to be able to rule on the spatiotemporal evolution of the desertification at the level of the basin of the Middle Moulouya between 1984 and 2022.

Conflict of interest the authors declare that there is no conflict of interest.

6   References

Adger WN, Benjaminsen TA, Brown K, Svarstad H (2001) Advancing a political ecology of global environmental discourses. Dev Change 32:681–715

Afrasinei G-M, Melis MT, Buttau C, et al (2017) Classification methods for detecting and evaluating changes in desertification-related features in arid and semiarid environments. Euro-Mediterranean J Environ Integr 2:1–19

Afrasinei GM, Melis MT, Arras C, et al (2018) Spatiotemporal and spectral analysis of sand encroachment dynamics in southern Tunisia. Eur J Remote Sens 51:352–374

Albalawi EK, Kumar L (2013) Using remote sensing technology to detect, model and map desertification: A review. J Food, Agric Environ 11:791–797

Badreldin N, Frankl A, Goossens R (2014) Assessing the spatiotemporal dynamics of vegetation cover as an indicator of desertification in Egypt using multi-temporal MODIS satellite images. Arab J Geosci 7:4461–4475

Becerril-Piña R, Díaz-Delgado C, Mastachi-Loza CA, González-Sosa E (2016) Integration of remote sensing techniques for monitoring desertification in Mexico. Hum Ecol Risk Assess An Int J 22:1323–1340

Benbrahim KF, Ismaili M, Benbrahim SF, Tribak A (2004) Problèmes de dégradation de l'environnement par la désertification et la déforestation: impact du phénomène au Maroc. Sci Chang planétaires/Sécheresse 15:307–320

Benmohammadi A, Benmohammadi L, Ballais J-L, Riser J (2001) Analyse des inter-relations anthropiques et naturelles: leur impact sur la recrudescence des phénomènes d'ensablement et de désertification au sud-est

du Maroc (vallée de Drâa et vallée de Ziz). Sci Chang planétaires/Sécheresse 11:297–308

Brandt CJ, Thornes JB (1996) Mediterranean desertification and land use.

Carlson TN, Ripley DA (1997) On the relation between NDVI, fractional vegetation cover, and leaf area index. Remote Sens Environ 62:241–252

Collado AD, Chuvieco E, Camarasa A (2002) Satellite remote sensing analysis to monitor desertification processes in the crop-rangeland boundary of Argentina. J Arid Environ 52:121–133

Dao PD, Liou Y-A (2015) Object-based flood mapping and affected rice field estimation with Landsat 8 OLI and MODIS data. Remote Sens 7:5077–5097

DAROUICHE FZ, ASSAOUD S, OUARHACHE D La dynamique de la désertification dans le Nord-Est du Maroc au cours des deux dernières décennies: Etat des lieux et précision des zones d'intérêt. Mots du Com d'organisation 228

Dregne HE (1986) Desertification of arid lands. In: Physics of desertification. Springer, pp 4–34

Dregne HE (2002) Land degradation in the drylands. Arid L Res Manag 16:99–132

Feng J, Ding JL, Wei WY (2018) A Study of soil salinization in Weigan and Kuqa rivers oasis based on Albedo-MSAVI feature space. China Rural Water Hydropower 2:147–152

Ghanam M (2003) La désertification au Maroc-Quelle stratégie de lutte. In: 2nd FIG Regional Conference Marrakech. pp 2–5

Guang Y, Dong C, Xinlin H, et al (2017) Land use change characteristics affected by water saving practices in Manas River Basin, China using Landsat satellite images. Int J Agric Biol Eng 10:123–133

Guo B, Zang W, Han B, et al (2020) Dynamic monitoring of desertification in Naiman Banner based on feature space models with typical surface parameters derived from LANDSAT images. L Degrad Dev

Hammouzaki Y (2013) Desertification and its control in Morocco. In: Combating Desertification in Asia, Africa and the Middle East. Springer, pp 91–111

HassaniM E, Douiri EM, Bammi J, et al (2013) Plantes médicinales de la Moyenne Moulouya (nord-est du Maroc). Ethnopharmacologia 50:39

Helldén U, Tottrup C (2008) Regional desertification: A global synthesis. Glob Planet Change 64:169–176

Herrmann S, Diouf AA, Sall I (2020) Beyond bioproductivity: Engaging local perspectives in land degradation monitoring and assessment. J Arid Environ 173:104002

Hostert P, Roder A, Jarmer T, et al (2001) The potential of remote sensing and GIS for desertification monitoring and assessment. Ann Arid Zone 40:103–140

Houlidi J, Benaabida L, El Jaafari S (2004) IMPACT DE LA DESERTIFICATION SUR LES SYSTEMES D'IRRIGATION DANS LA PLAINE DE TAFILALT. Le J l'Eau l'Environnement 3:52–60

Hu Y, Han Y, Zhang Y (2020) Land desertification and its influencing factors in Kazakhstan. J Arid Environ 180:104203

Huang Q, Cai Y (2009) Mapping karst rock in Southwest China. Mt Res Dev 29:14–20

Huang S, Siegert F (2006) Land cover classification optimized to detect areas at risk of desertification in North China based on SPOT VEGETATION imagery. J Arid Environ 67:308–327

Huete AR, Miura T, Gao X (2003) Land cover conversion and degradation analyses through coupled soil-plant biophysical parameters derived from hyperspectral EO-1 Hyperion. IEEE Trans Geosci Remote Sens 41:1268–1276

Kaemmerer M, Revel JC, Lefevre D (1990) DISSOLUTION EN CUVETTE ET ARASEMENT D'ELE-MENTS GROSSIERS CALCAIRES DANS DES CALCRE-TES, SUR DES FORMATIONS ALLUVIALLES QUATER-NAIRES (BASSIN DE KSABI, MOYENNE MOULOUYA, MAROe). Pédologie 123

Khiry MA (2007) Spectral mixture analysis for monitoring and mapping desertification processes in semi-arid areas in North Kordofan State, Sudan

Kosmas C, Kairis O, Karavitis C, et al (2014) Evaluation and selection of indicators for land degradation and desertification monitoring: methodological approach. Environ Manage 54:951–970

Lam DK, Remmel TK, Drezner TD (2010) Tracking desertification in California using remote sensing: A sand dune encroachment approach. Remote Sens 3:1–13

Lamchin M, Lee J-Y, Lee W-K, et al (2016) Assessment of land cover change and desertification using remote sensing technology in a local region of Mongolia. Adv Sp Res 57:64–77

Lamqadem AA, Saber H, Pradhan B (2018) Quantitative assessment of desertification in an arid Oasis using remote sensing data and spectral index techniques. Remote Sens 10:1862

LI H, LIU S (2003) A Model of Grassland Degradation Assessment Based on NDVI---Taking the Grassland in Tibet as an Example [J]. J Mt Res S 1:

Li J, Yang X, Jin Y, et al (2013) Monitoring and analysis of grassland desertification dynamics using Landsat images in Ningxia, China. Remote Sens Environ 138:19–26

Li Q, Zhang C, Shen Y, et al (2016) Quantitative assessment of the relative roles of climate change and human activities in desertification processes on the Qinghai-Tibet Plateau based on net primary productivity. Catena 147:789–796

Liang S (2001) Narrowband to broadband conversions of land surface albedo I: Algorithms. Remote Sens Environ 76:213–238

Liang S, Shuey CJ, Russ AL, et al (2003) Narrowband to broadband conversions of land surface albedo: II. Validation. Remote Sens Environ 84:25–41

Linli C, Wenyi F, Jun S, Gao Z (2006) Assessment of aeolian desertification in Korqin Sand, China. In: Remote Sensing and Modeling of Ecosystems for Sustainability III. International Society for Optics and Photonics, p 62981L

Liu Q, Liu G, Huang C (2018) Monitoring desertification processes in Mongolian Plateau using MODIS tasseled cap transformation and TGSI time series. J Arid Land 10:12–26

Louis J, Debaecker V, Pflug B, et al (2016) Sentinel-2 Sen2Cor: L2A processor for users. In: Proceedings Living Planet Symposium 2016. Spacebooks Online, pp 1–8

Ma Z, Xie Y, Jiao J, Wang X (2011) The construction and application of an Aledo-NDVI based desertification monitoring model. Procedia Environ Sci 10:2029–2035

Meng D, Zhang Z, Yang T, et al (2007) Research on dynamic evolvement of desertification in Beijing and its neighboring areas by remote sensing. In: 2007 IEEE International Geoscience and Remote Sensing Symposium. IEEE, pp 699–701

Middleton N, Thomas D (1997) World atlas of desertification.. ed. 2. Arnold, Hodder Headline, PLC

Mokhtari N (2016) ETUDE DE LA DYNAMIQUE DE LA DESERTIFICATION DANS LE BASSIN VERSANT DE LA MOULOUYA EN INTEGRANT LES DONNEES ISSUES DE LA

TELEDETECTION ET LES DONNEES SOCIO-ECONOMIQUES

Nkonya E, Mirzabaev A, Von Braun J (2016) Economics of land degradation and improvement–a global assessment for sustainable development. Springer Nature

Pan J, Li T (2013) Extracting desertification from Landsat TM imagery based on spectral mixture analysis and Albedo-Vegetation feature space. Nat hazards 68:915–927

Pannenbecker A (2006) Identification of desertification indicators using bi-temporal change detection. Cent Remote Sens L Surfaces 28:30

Pu R, Gong P, Michishita R, Sasagawa T (2008) Spectral mixture analysis for mapping abundance of urban surface components from the Terra/ASTER data. Remote Sens Environ 112:939–954

Qi J, Chehbouni A, Huete AR, et al (1994) A modified soil adjusted vegetation index. Remote Sens Environ 48:119–126

Ren YQ, Liu HL, Tang LX, et al (2014) A study on dynamic changes of desertification in south edge of Junggar basin based on NDVI-Albedo features. Bull Soil Water Conserv 34:267–271

Reynolds JF, Maestre FT, Huber-Sannwald E, et al (2005) Aspectos socioeconómicos y biofísicos de la desertificación. Ecosistemas 14:

Reynolds JF, Smith DMS, Lambin EF, et al (2007) Global desertification: building a science for dryland development. Science (80-) 316:847–851

Robinove CJ, Chavez Jr PS, Gehring D, Holmgren R (1981) Arid land monitoring using Landsat albedo difference images. Remote Sens Environ 11:133–156

Saadi O, Nouayti N, Nouayti A, et al (2021) Application of remote sensing data and geographic information system for identifying potential areas of groundwater storage in middle Moulouya Basin of Morocco, Groundwater for Sustainable Development, 14, 100639

SEGHIR A, MAZOZ L, IDRISSI AJ (2019) Cartographie de sol dans la zone méridional de la plaine de Tafrata au Maroc Centro-Oriental et évaluation de leur sensibilité à la désertification. Rev Marocaine des Sci Agron Vétérinaires 7:

Sun G, Chen X, Ren J, et al (2017) Stratified spectral mixture analysis of medium resolution imagery for impervious surface mapping. Int J Appl earth Obs Geoinf 60:38–48

Tag B (2003) Éspace et société agro-pastorale en mutation: dans le Maroc oriental steppique

UNCCD (2004) Preserving our common ground. UNCCD: 10 Years On. United Nations Convention to Combat Desertification Bonn, Germany

UNCCD UNC to CD (2015) Climate change and land degradation: Bridging Knowledge and Stakeholders

UNEP (1994) Development of guidelines for assessment and mapping of desertification and degradation in Asia/Pacific. In: Proceedings of the Draft Report of the Expert Panel Meeting, Paris, France, 17 June 1994. United Nations Environment Programme Robbie, Kanyana

Verbist K, Santibañez F, Gabriels D, Soto G (2010) Atlas de zonas áridas de América Latina y El Caribe

Veron SR, Paruelo JM, Oesterheld M (2006) Assessing desertification. J Arid Environ 66:751–763

Verstraete MM, Pinty B (1996) Designing optimal spectral indexes for remote sensing applications. IEEE Trans Geosci Remote Sens 34:1254–1265

Wang S, Grant RF, Verseghy DL, Black TA (2002) Modelling carbon dynamics of boreal forest ecosystems using the Canadian Land Surface Scheme. Clim Change 55:451–477

Wang T, Yan CZ, Song X, Xie JL (2012) Monitoring recent trends in the area of aeolian desertified land using Landsat images in China's Xinjiang region. ISPRS J Photogramm Remote Sens 68:184–190

Wang Y, Yan X (2017) Climate change induced by Southern Hemisphere desertification. Phys Chem Earth, Parts A/B/C 102:40–47

Wei H, Wang J, Cheng K, et al (2018) Desertification information extraction based on feature space combinations on the Mongolian plateau. Remote Sens 10:1614

Wei H, Wang J, Han B (2020) Desertification Information Extraction Along the China–Mongolia Railway Supported by Multisource Feature Space and Geographical Zoning Modeling. IEEE J Sel Top Appl Earth Obs Remote Sens 13:392–402

Wu Z, Lei S, Bian Z, et al (2019) Study of the desertification index based on the albedo-MSAVI feature space for semi-arid steppe region. Environ Earth Sci 78:232

Xiao J, Shen Y, Tateishi R, Bayaer W (2006) Development of topsoil grain size index for monitoring desertification in arid land using remote sensing. Int J Remote Sens 27:2411–2422

Xiaodong G, Jinren N, Zhenshan L, et al (2013) Quantifying the synergistic effect of the precipitation and land use on sandy desertification at county level: a case study in Naiman Banner, northern China. J Environ Manage 123:34–41

Xu D, Kang X, Qiu D, et al (2009) Quantitative assessment of desertification using Landsat data on a regional scale–a case study in the Ordos Plateau, China. Sensors 9:1738–1753

Xue Z, Qin Z, Li H, et al (2013) Evaluation of aeolian desertification from 1975 to 2010 and its causes in northwest Shanxi Province, China. Glob Planet Change 107:102–108

Yassoglou NJ, Kosmas C (2000) Desertification in the Mediterranean Europe. A case in Greece. RALA Rep 27–33

Yu H, Lee J-Y, Lee W-K, et al (2013) Feasibility of vegetation temperature condition index for monitoring desertification in Bulgan, Mongolia. Korean J Remote Sens 29:621–629

Yu P, Han D, Liu S, et al (2018) Soil quality assessment under different land uses in an alpine grassland. Catena 171:280–287

Zanchetta A, Bitelli G, Karnieli A (2016) Monitoring desertification by remote sensing using the Tasselled Cap transform for long-term change detection. Nat hazards 83:223–237

Zhao H-L, Li J, Liu R-T, et al (2014) Effects of desertification on temporal and spatial distribution of soil macro-arthropods in Horqin sandy grassland, Inner Mongolia. Geoderma 223:62–67

ZHAO H, LIU R, ZHOU R, et al (2013) Properties and mechanisms of change of soil macro-fauna communities in the desertification process of Horqin sandy grassland. Acta Prataculturae Sin 22:70